Available online at www.sciencedirect.com
SCIENCE DIRECT®
Catalysis Today 86 (2003) 73–85
CATALYSIS TODAY
www.elsevier.com/locate/cattod

Silica–alumina-supported transition metal sulphide catalysts for deep hydrodesulphurization

B. Pawelec [a], R.M. Navarro [a], J.M. Campos-Martin [a], A. López Agudo [a], P.T. Vasudevan [b], J.L.G. Fierro [a,*]

[a] *Institute of Catalysis and Petrochemistry, CSIC, Cantoblanco, 28049 Madrid, Spain*
[b] *Department of Chemical Engineering, University of New Hampshire, Durham, NH 03824, USA*

Received 5 February 2003; received in revised form 17 April 2003; accepted 21 April 2003

Abstract

Deep hydrodesulphurization (HDS) of dibenzothiophene (DBT) and gas-oil has been carried out on amorphous-silica–alumina (ASA)-supported transition metal sulphides (TMS) under conditions which approach industrial practice. The activity and selectivity of the binary Ni-, Ru- and Pd-promoted Mo catalysts were compared with the monometallic ones (Ru, Ir, Pd, Ni, Mo on ASA). For both HDS of DBT and gas-oil, the observed activity trends were similar; thus, all catalysts were more active with model feed than with gas-oil, and less active than commercial $CoMo/Al_2O_3$. The binary catalysts showed larger activity than monometallic ones, with Ni–Mo catalyst being more effective than Ru–Mo or Pd–Mo. For Ni–Mo sample, the X-ray photoelectron and temperature-programmed reduction techniques confirmed that incorporation of Mo minimises metal–support interaction, although the formation of nickel hydrosilicate was not prevented. The consecutive impregnation of calcined Mo/ASA catalyst with precursor solution followed by calcination enhances molybdenum surface exposure in binary samples. As a consequence, the temperature of reduction of MoO_3 to molybdenum suboxides is decreased.

Keywords: Deep hydrodesulphurization; DBT; Gas-oil; Transition metal sulphides

1. Introduction

Reduction of sulphur in fuels is a pressing environmental concern, and the Environmental Protection Agency (EPA) has proposed new guidelines to limit the sulphur in diesel fuels to less than 15 ppm beginning in 2006. In order to meet these stringent specifications, deep HDS of diesel fuel requires the use of novel catalysts.

Hydrotreating reactions such as hydrodesulphurization (HDS), hydrodenitrogenation (HDN) and hydrocracking (HC) are conventionally conducted on cobalt (or nickel) molybdenum catalysts supported on carriers which are more or less acidic depending on the function to be promoted [1]. As pointed out in literature [1–7], the support has a marked effect on the specific activity of the sulphide catalysts.

Alumina-supported catalysts exhibit good performance in HDS and HDN reactions but only a moderate cracking activity. For this reason, in the new generation of hydrotreating catalysts, both the nature of the support and/or the active phase have been varied. A good alternative to alumina support is amorphous-silica–alumina (ASA) since it displays greater acidity [3,4,8]. Although a high acidity of ASA support tends

* Corresponding author. Fax: +34-915854760.
E-mail address: jlgfierro@icp.csic.es (J.L.G. Fierro).

0920-5861/$ – see front matter © 2003 Elsevier B.V. All rights reserved.
doi:10.1016/S0920-5861(03)00405-X

to enhance coking [4], catalysts supported on ASA have the advantage of low metal–support interaction compared to those supported on alumina. On the one hand, strong metal–support interaction (SMSI) makes it easy to prepare highly dispersed MoS_2, which remains stable during the reaction; on the other hand, it induces the formation of new surface species through solid-state reactions of promoter and molybdenum oxide at the alumina interface, which is undesirable. These latter species becomes difficult to sulphide, and therefore these catalysts show lower HDS activity. However, minimising the metal–support interaction in catalysts by using silica–alumina as carriers (by increasing the SiO_2 content), also leads to a decrease in HDS and hydrogenation (HYD) activity [4–6,8–10]. The poor dispersion of active phases has usually been described as the principal reason for lower activity, because the silica–alumina support with high silica loadings exhibits a lower number of basic –OH groups that have the potential to react with molybdates during impregnation [7].

Since the classical study of Pecoraro and Chianelli [11] on unsupported transition metal sulphides (TMS) that demonstrated the variation of DBT HDS activity with the position of the elements in the periodic table, published work in the field of deep desulphurisation over supported TMS has seen a tremendous increase in recent years [9,12–23]. Application of ASA-supported noble-metal catalysts in the deep HDS of diesel fuel was extensively studied by Moulijn and co-workers [17–19] and van Santen and co-workers [20–22], and in our laboratory using a model feed [12–15]. For diesel fuel, it was found that the Pt/ASA catalyst showed comparable activity to Ni–W/γ-Al_2O_3 catalyst which was higher than that of the conventional Co–Mo/γ-Al_2O_3 catalyst [17–20]. Employing dibenzothiophene [12–15] as model compound, Pt/ASA catalyst (provided by Shell) was found to exhibit the highest HDS activity also. The better performance of Pt/ASA in the HDS of model feeds as compared to diesel fuel was attributed by Reinhoudt et al. [17] to poisoning of part of the active phase by basic nitrogen compounds like quinoline.

In view of the observed discrepancies between the catalytic activity for model and real feeds, this article compares the activities of the ASA-supported monometallic TMS (Ru, Pd, Ir, Mo, Ni) and bimetallic Ru-, Ni- and Pd-promoted Mo sulphide catalysts for the HDS of DBT and diesel fuel. In the case of binary M–Mo catalysts, the objective was to cover the ASA surface as much as possible by incorporating large amounts of MoO_3 prior to promoter addition. Thus, the molybdenum sulphide phase, in addition to its role in enhancing activity, should be regarded as a support for the promoter, enabling the promoter to be optimally dispersed.

2. Experimental

2.1. Catalyst preparation

An amorphous-silica–alumina (ASA) (Si/Al = 0.62 atomic ratio, surface area 389 $m^2\,g^{-1}$, pore volume 0.72 $ml\,g^{-1}$) was used as support. The monometallic catalysts were prepared by contacting the ASA (particle size of 0.25–0.30 mm) with 50 ml of metal precursor solution at a pH close to 7. For preparation of Mo, Ru, Ir, Pd and Ni catalysts, the precursors employed were: $(NH_4)_6Mo_7O_{24}{\cdot}H_2O$ (Merck, reagent grade), $RuCl_3$ (Sigma), $IrCl_3{\cdot}3H_2O$ (Alfa), $Pd(NO_3)_2{\cdot}2H_2O$ (Fluka) and $Ni(NO_3)_2{\cdot}6H_2O$ (Merck). After contacting ASA support with the impregnating solution for 12 h, the excess water was removed in a rotary evaporator, then the precursors were dried at 383 K for 4 h and calcined in a two-step procedure: first at a rate of 4 K min^{-1} to 523 K and maintaining this temperature for 1 h, and then raising temperature to 723 K followed by isothermal calcination at that temperature for 2 h.

The binary M–Mo/ASA (M = Ru, Pd, Ni) catalysts were prepared by impregnation of the Mo/ASA with aqueous solutions of $RuCl_3$ (Sigma), $Pd(NO_3)_2{\cdot}2H_2O$ (Fluka) and $Ni(NO_3)_2{\cdot}6H_2O$ (Merck), respectively. The excess water was removed in a rotary evaporator and the impregnates were dried at 373 K in air for 4 h, and calcined at 573 K for an additional 4 h. The final metal content in all catalysts, as determined by atomic absorption spectroscopy, is compiled in Table 1.

2.2. Characterisation techniques

Metal contents were determined by atomic absorption spectrometry using a Perkin-Elmer 3030 absorption instrument. The samples were solubilised in a solution of HF, HCl and HNO_3 and homogenised

Table 1
Some characterisation data of calcined ASA-supported catalysts

Catalyst	M[a] (wt.%)	Pore diameter[b] (nm)	BET[b] ($m^2\ g_{cat}^{-1}$)	TPR[c] (T_{max}, K)
ASA	–	6.8	389	923
Ru	0.78	7.2	358	471
Pd	0.98	7.1	372	293, 320, 354
Ir	0.68	7.2	347	505
Ni	5.7	6.4	359	650, 760, 848
Mo	16.1	7.6	156	733[d], 973
Ru–Mo	0.87	6.9	290	454, 693[c], 962
Pd–Mo	0.92	7.3	282	678[c], 1004
Ni–Mo	1.60	7.7	283	688[c], 1034

[a] Metal loading as determined by atomic absorption spectroscopy; for monometallic samples, M represents the following metals: Ru, Pd, Ir, Ni and Mo for Mo sample; for binary samples the Mo content was close to those reported for Mo sample.
[b] Specific area and average pore diameter (d_p) as measured by N_2 adsorption isotherms at 77 K.
[c] T_{max} determined by temperature-programmed reduction.
[d] Peak indicative of the reduction of Mo^{6+} to Mo^{4+}.

in a microwave oven. The calcined samples were characterised by X-ray diffractometry according to the step-scanning procedure (step size 0.02°; 0.5 s) with a computerised Seifert 3000 diffractometer using Cu Kα ($\lambda = 0.15406$ nm) radiation and a PW 2200 Bragg–Brentano $\theta/2\theta$ goniometer equipped with a bent graphite monochromator and an automatic slit. The nitrogen adsorption–desorption isotherms of the calcined samples were obtained at 77 K over the whole range of relative pressures using a Micromeritics Digisorb 2600 automatic equipment on samples previously outgassed at 523 K. BET specific areas were computed from these isotherms using the BET method.

Temperature-programmed reduction (TPR) profiles were obtained on a semiautomatic Micromeritics TPD/TPR 2900 apparatus interfaced with a computer. The sample of 0.050 g was housed in a quartz tubular reactor and the TPR profiles were obtained by passing a 10% H_2/Ar (Air Liquide, 99.996%) flow (60 ml min^{-1}) through the sample at temperatures from 303 to 1173 K. The temperature was increased at a rate of 15 K min^{-1} and the amount of H_2 consumed was determined with a thermal conductivity detector (TCD). A cooling trap placed between the sample and TCD was used to retain the water produced during the reduction process.

FTIR spectra of adsorbed pyridine were recorded in order to evaluate the acidity of sulphided samples. Samples, in the form of self-supporting wafers of ca. 12 mg cm^{-2}, were pre-treated in an infrared cell designed to work either under vacuum or in dynamic conditions and fitted with greaseless stopcocks and KBr windows. Details on the procedure have been described elsewhere [14].

X-ray photoelectron spectra (XPS) of the used catalysts were recorded on a VG Escalab 200R electron spectrometer equipped with a hemispherical electron analyser, using a Mg Kα ($h\nu = 1253.6$ eV, 1 eV = 1.603×10^{-19} J) X-ray source. The ECLIPSE software was used to record and analyse spectra. The procedure followed to measure binding energies (BE) and relative proportion of catalyst constituents of sulphided samples has been described elsewhere [13,14]. The core-level spectra of the transition element and also that of S 2p, Si 2p and Al 2p were recorded and the corresponding BE by referencing to the C 1s line at 284.9 eV (accuracy within ±0.1 eV).

2.3. Activity tests

The HDS reaction of DBT model compound was performed in a high-pressure laboratory scale set-up equipped with a stainless-steel fixed bed catalytic reactor (9.5 mm i.d. and 130 mm length). DBT was dissolved in decalin to obtain a 1 wt.% solution. For the activity tests, 0.3 g of the catalyst with particle size 0.25–0.3 mm was used. The activation procedure consisted of heating to the sulphidation temperature of 673 K in N_2 flow at atmospheric pressure followed by sulphidation in a H_2:H_2S mixture (ratio 10:1) at 673 K for 4 h, then purging under a N_2 flow at 673 K for 1 h.

Before the run, the N_2 pressure was increased up to 3 MPa and the catalytic bed was heated to the desired experimental temperature. The reaction conditions for the HDS of DBT were: temperature 523–593 K; total pressure 3 MPa; H_2 flow rate 7 l(STP) h^{-1} and WHSV = 35 h^{-1}. Liquid samples were analysed by GC (Varian chromatograph Model Star 3400 CX) equipped with a 30 m × 0.53 mm column with DB-1 (100% methyl-polysiloxane, J&W Scientific) as stationary phase, using an initial temperature of 313 K (for 1 min) and then heating at a rate of 18 K min^{-1} up to 473 K and holding at that temperature for 5 min.

Activity was measured at four different temperatures: 523, 553, 573 and 593 K running from the lowest to the highest temperature and maintaining the reaction for 1 h at each temperature. At each temperature, the purge of the liquid reservoir was carried out for 45 min, and then the liquid effluent was collected for 15 min and analysed. Each value of total conversion is the average of three different analyses of the liquid product taken after 1 h on-stream at a given temperature. Once the reaction was carried out at a given temperature, the next temperature was reached while maintaining the catalyst in a flow of inert gas. In order to check if there was any deactivation of the catalysts, the activity was checked back at the lowest temperature (523 K) at the end of all the experimental runs. In addition to unreacted DBT, biphenyl (BP) and cyclohexylbenzene (CHB) were the only products detected. Total DBT conversion was calculated as DBT disappearance and HDS and HYD selectivities were defined as (BP)/(CHB + BP) × 100 and (CHB)/(CHB + BP) × 100, respectively. For the calculation of HYD a sequential path was assumed (DBT → BP → CHB). The other pathway is neglected because the products 1,2,3,4-tetra hydrodibenzothiophene (THDBT) and 1,2,3,4,5,6-hexahydrodibenzothiophene (HHDBT) were not observed. Also the product DCH was not observed.

The activity of the catalysts in deep HDS of gas-oil was evaluated in a continuous flow micro-reactor at constant temperature (623 K) and pressure (3 MPa) using 0.2 g of catalyst (particle size 0.25–0.30 mm) diluted 1:5 volume with SiC particles. Hydrotreated gas-oil (610 ppm S that is mostly present as alkyl-substituted DBTs, and 160 ppm of N) was used as a feedstock. Prior to the reaction, the catalysts were pre-sulphided in situ with a mixture of 7 vol.% CS_2 in gas-oil at 623 K and 2 MPa for 4 h. After catalyst sulphiding, the pressure of the system was increased up to 3 MPa and the sulphiding mixture substituted by the hydrotreated feed. In each test run, a stabilisation period of 2 h on-stream was allowed before the first liquid sample was taken. Two successive samples of liquid collected during 30 min were taken for analysis. In order to test catalyst stability, the test run was repeated at the next day under the same operating conditions. Between experiments the catalyst was kept under H_2 pressure (>0.5 MPa) at room temperature. The amount of sulphur in the feedstock and in products was determined with an Antek analyser.

3. Results

3.1. Activity tests

For model feed, the activity data of sulphided M/ASA and M–Mo/ASA (M = Ru, Pd, Ir, Ni, Mo) catalysts (expressed as total DBT conversion) as a function of the reaction temperature are displayed in Fig. 1. As expected, the conversion of DBT increased progressively with temperature. For Ni–Mo, the

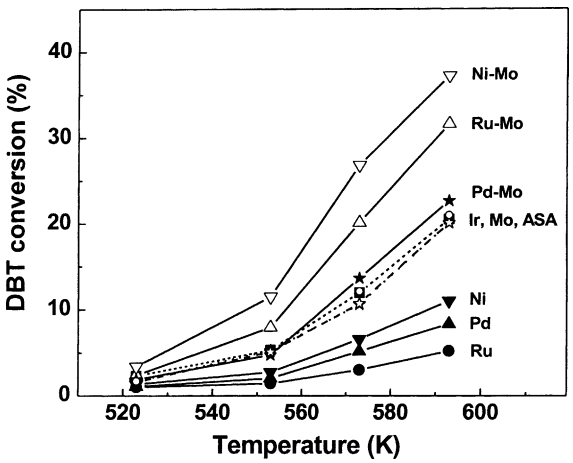

Fig. 1. Dependence of the overall DBT conversion on the reaction temperature for M/ASA (M = Ru, Pd, Ni, Mo and Ir), and M–Mo/ASA catalysts (M = Pd, Ru, Ni). The ASA support is also included for comparison. Reaction conditions were: T = 523–593 K, P = 3 MPa and WHSV = 47 h^{-1}.

synergy effect was larger at 573 K than at 593 K. Thus, DBT conversion on the binary Ni–Mo catalyst at 573 K is approximately 56% higher than the sum of DBT conversions on the Ni and Mo monometallic catalysts, whereas this increase is only by about 11.8% at 593 K. Clearly, the most striking result is the similar activity of the blank ASA and Mo samples despite the large Mo loading of the latter catalyst (16.1%). The low activity of Mo catalyst could be due, in part, to the strong decay of its BET area. For this reaction, very little deactivation of any of the catalysts was observed (data not presented); the activity checked at the end of a complete run at different temperatures was almost unchanged. For HDS of DBT at 593 K, the observed activity trend is: commercial $CoMo/Al_2O_3 \gg$ Ni–Mo > Ru–Mo > Pd–Mo > ASA ≈ Ir ≈ Mo > Ni > Pd > Ru. Considering the activity profiles in the hydrodesulphurization of DBT on bulk transition metal sulphides [11], this trend on ASA-supported catalysts is surprising because the ASA carrier alone shows higher activity than other sulphided metals (Ir, Mo, Ni, Pd and Ru). As expected, the monometallic samples display lower activity than binary M–Mo formulations, in good agreement with literature [24].

For HDS of gas-oil and DBT, the comparison of the activity data of sulphided ASA-supported samples with those of commercial $CoMo/Al_2O_3$ catalyst are displayed in Figs. 2 and 3, respectively. In general, the

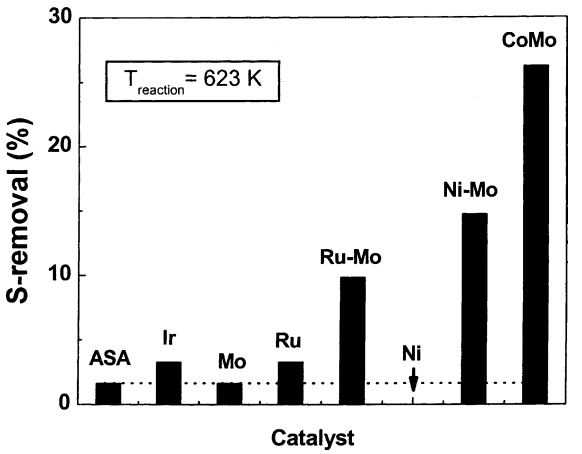

Fig. 2. Effect of catalyst composition on gas-oil HDS at 623 K and $P = 3$ MPa.

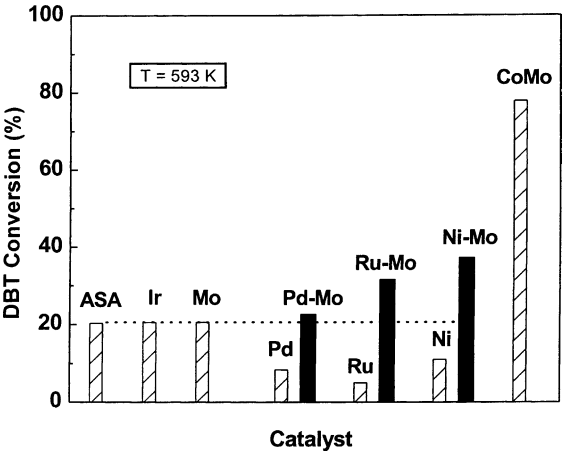

Fig. 3. Effect of catalyst composition on total DBT conversion at 593 K ($P = 3$ MPa, WHSV $= 47\ h^{-1}$).

activity trends in HDS of gas-oil and DBT are similar. For both HDS of DBT and gas-oil, Ni appears to be the best promoter among the binary catalysts. Noticeably, the differences between Ru–Mo and Ni–Mo are lower for HDS of DBT than for gas-oil.

The influence of reaction temperature on HYD selectivity in the conversion of DBT is presented in Fig. 4. From this figure, it appears that for all catalysts studied, the C–S bond cleavage (HLS) reaction of DBT is dominant over hydrogenation of aromatics rings, which agrees with previous findings [25–27]. From Fig. 4, the trend of HYD at 593 K is: Pd–Mo > Ru–Mo ≈ Mo > Pd > Ru > ASA > Ni > Ni–Mo ≈ Ir, whereas for HLS the trend is opposite (HLS + HYD = 100%). Contrary to Ru and Ni promoters, it was found that incorporation of Pd to the Mo catalyst leads to an increase in the hydrogenation capability of Mo catalyst by a factor of two only at 520 K, not at higher temperatures. At 593 K, the HDS selectivity of the Ni–Mo and Ir samples is the largest among catalysts studied (ca. 97%). In agreement with thermodynamic calculations [26,27], it is observed that the hydrogenation selectivity for Pd, Ru, Ni, Ir and Ni–Mo catalysts decreases with increasing reaction temperature. However, for Pd–Mo, Mo and Ru–Mo catalysts, an increase in hydrogenation selectivity with increasing reaction temperature (from 523 to 573 K) occurs. Further increase in temperature from 573 to 593 K led to a decrease in HYD

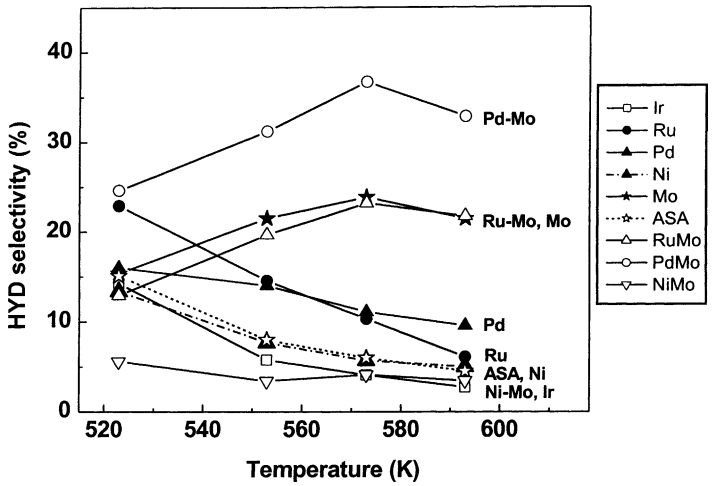

Fig. 4. Influence of reaction temperature on HYD selectivity in the HDS of DBT on M/ASA (M = Ir, Ru, Pd, Mo and Ni) and M–Mo/ASA (M = Ru, Pd, Ni) catalysts. Reaction conditions as in Fig. 1.

selectivity. This behaviour might indicate that at high reaction temperatures some thermodynamic effects are involved. Fig. 5 shows HYD selectivity vs. HDS of DBT reaction rate for M/ASA series. As can be seen, a drastic decrease in HYD selectivity occurs with increasing DBT reaction rate. This means that in the absence of thermodynamic effects, the hydrogenolysis of DBT is more favourable than hydrogenation of aromatics rings on M/ASA.

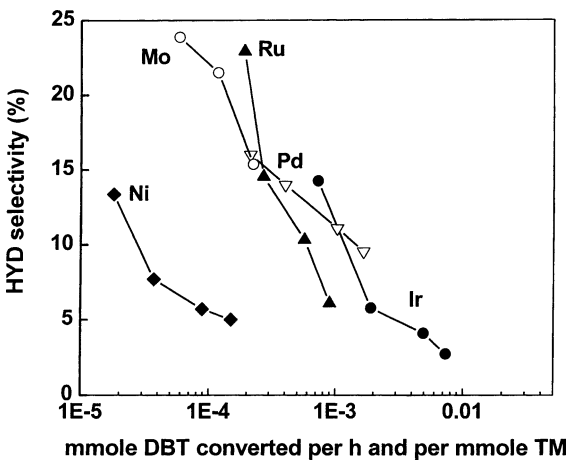

Fig. 5. Selectivity toward HYD products during HDS of DBT vs. intrinsic activity of ASA-supported catalysts calculated as millimole DBT converted per millimole of TM (TM = Ru, Pd, Ir, Ni, Mo) catalysts. Reaction conditions as in Fig. 1.

3.2. Composition, textural and structural properties of catalysts

Chemical composition and textural properties of the calcined catalysts are summarised in Table 1. For the monometallic ASA-supported catalysts the amount of transition metal oxides varied over a broad range (0.68–16.1 wt.%). The Ir and Mo catalysts showed the lowest and highest metal loading, respectively. For binary catalysts, the molybdenum content was very close to those of Mo base catalyst (16.1%). The BET areas and mean pore diameters are compiled in Table 1. For Ru, Pd, Ir and Ni catalysts, the BET area decreased only slightly upon metal incorporation. The strong decrease in BET specific area after Mo incorporation on ASA (from 389 to 156 $m^2 g^{-1}$), is expected as the support surface is covered by a high molybdenum amount (16.1 wt.%). Moreover, X-ray diffraction pattern of this sample showed diffraction lines of MoO_3 (JCPDS pattern 35-609) of crystal size 8.7 nm, and $Mo_{17}O_{47}$ phase (JCPDS pattern 13-345) of crystal size 9.3 nm. In the other monometallic and bimetallic catalysts, no crystalline phases were detected. In line with XRD data, the increase in BET specific area for binary samples suggests that MoO_3 crystals are redispersed along the second impregnation step, which agrees with previous observations [5].

In general, incorporation of one or two metals leads to an increase in the average pore diameter.

According to the IUPAC classification, the N_2 isotherms (not shown here) of the supported catalysts are of type IV, whereas their hysteresis loops belong to type H2 [28]. The hysteresis loop proved to be relatively large and appeared at low relative pressures, indicating the presence of mesopores. The average pore diameter of all catalysts was in range 6.4–7.7 nm.

3.3. Temperature-programmed reduction (TPR)

TPR experiments of ASA-supported catalysts were performed with the aim to obtain information about the metal–support interaction and to examine possible correlations between the reducibility of the oxidic precursor and HDS activity of the sulphided samples, as has been previously reported [29–31]. The TPR profiles of M (M = Ru, Pd, Ir, Ni, Mo) and M–Mo (M = Pd, Ru, Ni) catalysts are displayed in Fig. 6, and the reduction temperature maxima are compiled in Table 1. TPR profile of ASA, included for comparison, showed a hydrogen consumption peak at ca. 923 K, with a shoulder in the high temperature side (>973 K), probably due to reduction of some impurities usually present in the carrier. TPR profiles of the Ir and Ru samples showed sharp reduction peaks at 505 and 471 K indicative of reduction of iridium and ruthenium oxides, respectively. The TPR profile of Pd catalyst is more complicated since it exhibits two peaks around 290 and 320 K, indicative of reduction of Pd^{2+} to Pd^0 followed by H_2 chemisorption and absorption in Pd metal [32] as well as a negative peak around 354 K, which is produced by decomposition of Pd hydride [33]. TPR profile of Ni catalyst showed three peaks at 650, 760 and 848 K. Since it is known that Ni^{2+} species are reduced without the formation of intermediate oxides [34], the peak at 650 K is probably indicative of the reduction of "NiO" phases which resembles bulk nickel oxide in the form of large crystallites dispersed without chemical interaction by the ASA surface [35]. The higher temperature observed in this study (650 K) as compared to those reported for reduction of the bulk NiO (503 K) [36] reflects the polarisation effect of silica and aluminium ions. Considering the results of Mile et al. [35], the peak at 760 K can be ascribed to NiO in the form of crystallites as a result of nucleation. Finally, the peak with a maximum at 848 K can reasonably be ascribed to the formation of the nickel hydrosilicate species [37]. The presence of spinel-like structures could be excluded since all catalysts were calcined at 723 K, at which temperature, the diffusion of nickel ions into the support is limited.

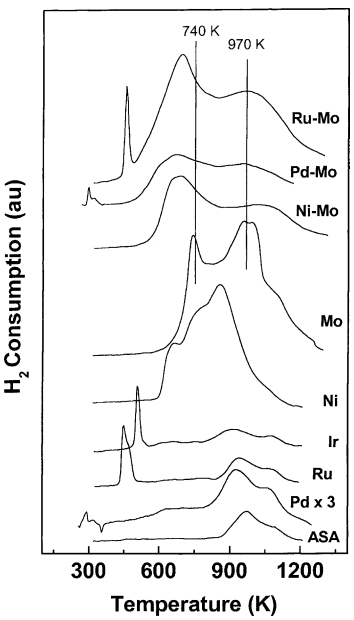

Fig. 6. TPR profiles of ASA-supported catalysts and blank ASA carrier.

Contrary to Ni, the reduction of supported MoO_3 species occurs in two steps ($MoO_3 \rightarrow MoO_2 \rightarrow Mo^0$). Thus, two peaks at 733 and 973 K observed in the TPR profile of Mo sample can be assigned to reduction of Mo^{6+} to Mo^{4+}, and to reduction of Mo suboxides to Mo^0, respectively. Note that for binary catalysts the peak from first step of MoO_3 reduction is shifted to lower reduction temperatures, in good agreement with literature [38,39]. For Ni–Mo sample, the peaks indicative of the two reduction steps of MoO_3 phase overlap with the peaks from the reduction of NiO and a nickel hydrosilicate phase. On the contrary, for Pd–Mo sample, the reduction of PdO to Pd^0 (peak at 293 K) occurs at a temperature much lower than the Mo oxides (peaks at 733 and 973 K). The formation of a palladium hydride is inhibited in this catalyst, which contrasts with formation of this phase in Pd sample. For Ru–Mo sample, the peak at 454 K, indicative of reduction of ruthenium oxide phase [40], is separate from the other two peaks of Mo oxide reduction (peaks at 733 and 973 K). The small differences in the

Table 2
Binding energies (eV) of core electrons in monometallic and bimetallic catalysts used in HDS of DBT[a] and gas-oil[b]

Catalyst	Mo 3d		M (inner level)[a]		Phases
Ru	–	–	281.2 (21)	279.9 (76)	RuS_2, Ru^0
			281.4 (42)	**279.7 (58)**	
Pd	–	–	336.9 (15)	335.4 (85)	PdS, Pd^0
Ir	–	–		60.8 (100)	Ir^0
				61.4 (100)	
Ni	–	–	853.8 (18)	856.7 (82)	NiS, Ni^{2+}
			854.1 (17)	**856.6 (83)**	
Mo	229.4 (80)	231.2 (20)	–	–	MoS_2, "OMoS"
	229.5 (74)	**232.0 (26)**			
Pd–Mo	229.3 (71)	231.2 (29)	336.9 (31)	335.7 (69)	MoS_2, "OMoS", PdS, Pd^{2+}
Ru–Mo	229.3 (81)	231.3 (19)	281.2 (37)	280.4 (63)	MoS_2, "OMoS", RuS_2, Ru^0
	229.3 (70)	**232.1 (30)**	**281.4 (52)**	**280.3 (48)**	
Ni–Mo	229.5 (51)	231.2 (49)	854.1 (63)	855.0 (37)	MoS_2, "OMoS", NiS, "NiO"
	229.3 (52)	**232.3 (48)**	**854.2 (43)**	**855.0 (57)**	

[a] M represents the following levels: Ir $4f_{7/2}$ for Ir, Pd $3d_{5/2}$ for Pd, Ni $2p_{3/2}$ for Ni and Ru $3d_{5/2}$ for Ru.
[b] Data in bold are catalysts used in gas-oil HDS.

reduction temperature observed for Ru and Ru–Mo are more likely due to changes in RuO_2 crystallite sizes.

3.4. Photoelectron spectroscopy

The chemical species present on the catalysts surface and their proportion were evaluated by XPS with the aim to explain the activity trends in HDS reactions of DBT and gas-oil. The BE of core-levels of the atoms in samples used in HDS of DBT and gas-oil are summarised in Table 2. For illustrative purpose, some spectra of representative catalysts used in HDS reactions of gas-oil are shown in Fig. 7. The Si 2p (ca. 102.9 eV) and Al 2p (ca. 74.7 eV) core-levels for all catalysts coincide with those of the ASA substrate. Similarly, the S 2p energy region showed a single component close to 162.3 eV, which is characteristic of sulphide (S^{2-}) species.

As can be seen in Fig. 7, the Ir 4f doublet of the sample used in HDS of gas-oil is well resolved and the major Ir $4f_{7/2}$ component appeared at a binding energy characteristic of metallic iridium. This observation agrees with the absence of iridium sulphide species after HDS of DBT (Table 2). For the other Pd, Ru, Ni and Mo monometallic catalysts the chemical nature of surface species is different. Thus, in the Pd catalyst used in HDS of DBT, the Pd $3d_{5/2}$ profile was deconvoluted into two components at 336.9 and 335.4 eV, which can be ascribed to PdS and Pd^0 species, respectively [41]. Similarly, the Ru catalyst used in HDS of DBT showed two components, a major one at 279.9 eV associated to Ru metal and a minor one at 281.2 eV due to RuS_2 species [42,43]. Interestingly, the fraction of ruthenium in the sulphide state was doubled when the Ru monometallic catalyst was employed in HDS of gas-oil (Table 2). For the Ni catalyst, the Ni $2p_{3/2}$ peak displays a minor contribution at ca. 854.0 eV, associated with sulphided Ni^{2+} ions [41], and another major one at around 856.6 eV, arising from Ni^{2+} ions in an environment of oxide ions [37]. In the bimetallic Ni–Mo catalyst, this last component is shifted from 856.7 to 855.0 eV, suggesting a weakening of the Ni–support interaction and formation of Ni species close to the oligomeric NiO phase as induced by presence of Mo [44].

The Mo 3d core-level spectra of all Mo catalysts used in HDS reactions of DBT and gas-oil were complex because of the overlapping contribution of the S 2s peak in the low BE region. Curve fitting procedures revealed the presence of two Mo 3d doublets: a major one with the Mo $3d_{5/2}$ peak at 229.4 eV is characteristic of MoS_2 species, and a minor one above 231.2 eV is due to unsulphided (Mo–O) and/or partially sulphided (O–Mo–S) species probably located at the support interface. No significant changes in the BE of Mo 3d peaks were found in the bimetallic M–Mo (M = Pd,

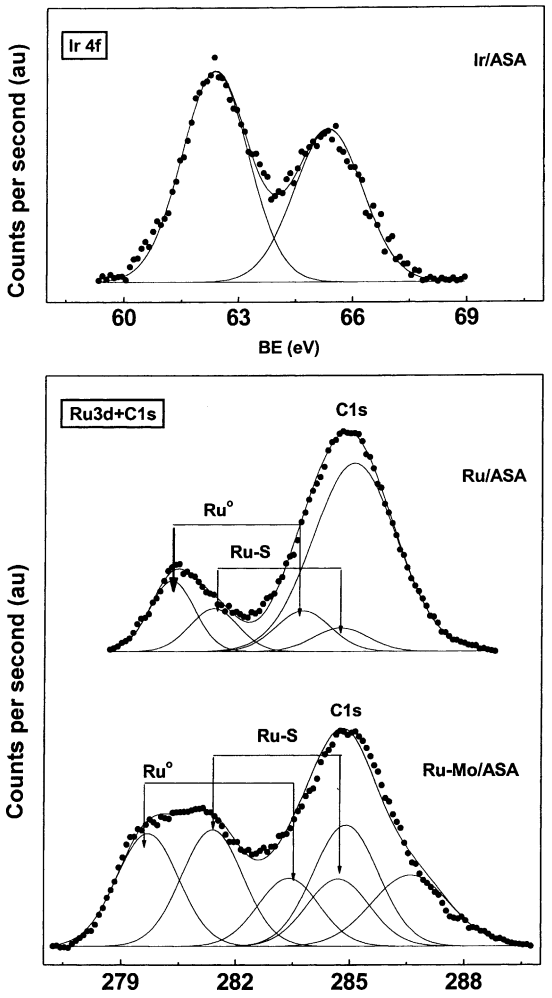

Fig. 7. XPS spectra of Ir/ASA, Ru/ASA and Ru–Mo/ASA catalysts after HDS of gas-oil.

Ru, Ni) systems. However, an examination of the peak percentages shows a lower fraction of molybdenum sulphide in the bimetallic Ni–Mo sample, and this is similar for HDS of DBT and gas-oil.

Surface atomic ratios were also calculated for the monometallic and bimetallic M–Mo used in HDS of DBT and gas-oil. A few of these quantitative data are collected in Table 3. In general, some changes in the M/Si ratios of the monometallic catalysts occurred after using the catalysts in both HDS reactions, although these changes became smooth in the bimetallic M–Mo catalysts.

Table 3
Acidity[a] and surface atomic ratios[b] of catalysts used in HDS reactions[c]

Catalyst	Brønsted/Lewis[a]	M/Si[b]		Mo/Si	
		DBT[c]	Gas-oil[d]	DBT[c]	Gas-oil[d]
ASA	0.12 (0.06)	–	–	–	–
Ru	0.08	0.31	0.27	–	–
Pd	0.07	0.19	nd	–	–
Ir	0.11	0.02	0.02	–	–
Ni	0.03	0.13	0.12	–	–
Mo	0.11	–	–	1.75	1.22 (0.14)[e]
Pd–Mo	0.06	0.27	nd	0.83	nd
Ru–Mo	0.10	0.30	0.27	0.83	0.94
Ni–Mo	0.10	0.10	0.12	0.91	0.97

[a] Brønsted-to-Lewis acidity ratio (I_{1549}/I_{1455}) of sulphided catalysts and bare carrier determined from the IR spectra of adsorbed pyridine; B/L acidity ratio determined for oxidic ASA is given in parenthesis.

[b] As determined by X-ray photoelectron spectroscopy.

[c] Reaction conditions were: $P = 3$ MPa, WHSV $= 47\,h^{-1}$ and $T = 593$ K.

[d] Reaction conditions were: $P = 3$ MPa; $T = 623$ K; nd: no determined.

[e] The Mo/Si ratio calculated by the Kerkhoff–Moulijn model for a monolayer [47].

3.5. Infrared spectroscopy of adsorbed pyridine

The relative proportion of Brønsted (B) and Lewis (L) acid sites, expressed as the ratio of the intensity of the bands at approximately 1543 and 1453 cm^{-1} [45], respectively, was determined with the aim to determine possible correlation between catalyst acidity and their catalytic response. Spectra of adsorbed pyridine on ASA confirmed the presence of Brønsted and Lewis acid sites (spectra not shown here). However, this acidity is mainly of the Lewis-type because ASA material used as carrier possesses only 28% of the alumina. Brønsted-to-Lewis acidity ratios of all catalysts are recompiled in Table 3. From these data the B/L acidity ratio follows the order: ASA $\approx$ Ir $\approx$ Mo $>$ Ni–Mo $\approx$ Ru–Mo $>$ Ru $>$ Pd $>$ Pd–Mo $>$ Ni. The changes in B/L acidity ratio in binary samples depend on the type of promoter. This is illustrated by the relatively high B/L acidity ratio of Ru–Mo and Ni–Mo catalysts, which contrasts with the very low B/L ratio of the Pd–Mo sample. Comparing the acidity of calcined and sulphided ASA, it appears that a strong enhancement in the B/L acidity ratio occurred upon sulphidation.

4. Discussion

4.1. Influence of the feed composition on catalyst performance

On looking at the catalysts' performance, it is evident that all the catalysts are more active with model feed than with pre-desulphurised gas-oil. The larger activity of the catalysts in the HDS reaction of the model feed can likely be due to differences in the catalyst activation procedure and also to feed composition. Thus, the catalyst employed in the HDS of model feed were activated in a H_2+H_2S gas mixture at 673 K prior to the reaction, while for the gas-oil feed, they were sulphided with CS_2 (7 vol.%) added to gas-oil feed deliberately. In this latter case, the catalyst sulphidation is less effective since the reaction operates under trickle-bed conditions and sulphidation becomes mass transfer limited. Support for this interpretation comes from the data provided by photoelectron spectroscopy of the catalysts used in HDS of both feeds (results not shown here). For the Mo and Ni monometallic and also for the Ru–Mo and Ni–Mo bimetallic systems, the surface S/M (M = Ni, Mo, Ru) ratios were always lower (10–18%) for the samples employed in the HDS of gas-oil than in the HDS of model feed.

Another possibility to be considered is the difference in the chemical nature of the two feeds. The sulphur compounds present in the pre-desulphurised gas-oil are highly refractory as most of them are alkyl-substituted benzothiophenes and dibenzothiophenes, which are very difficult to desulphurize [17–22]. In addition, while in the model feed N-containing compounds are not present, in the pre-desulphurised gas-oil used there remain some N-containing compounds at a concentration of 160 ppm. As these compounds are basic, they are strongly adsorbed on the acid sites of the support and supported phases, thus they act as poisons. This interpretation was advanced by Nagai and Kabe [46] who observed an important inhibition in the rate of S-removal upon dosing nitrogen-containing compound into the feed and then performing HDS reaction in a large range of temperatures. Additional support to this interpretation comes from the results of Reinhoudt et al. [17] related to the HDS reaction of a model feed and a pre-desulphurized diesel feed on an ASA-supported Pt catalyst. These authors also observed a drop in activity when using the diesel feed and ascribed it to partial poisoning of part of the active phase by basic nitrogen compounds like quinoline.

4.2. Catalyst structures

For the binary samples used in HDS of DBT, the percentages of the molybdenum sulphide species compiled in Table 2 and the molybdenum surface exposure expressed as Mo/Al atomic ratio (Table 3), follow the same sequence: Ru–Mo > Pd–Mo > Ni–Mo. This indicates that the enhancement in sulphidation degree of the molybdenum species occurs in parallel with the molybdenum surface exposure obtained after consecutive impregnation of the Mo/ASA base catalyst with the precursor solution of the transition metal. Since a contrary trend is shown in the overall DBT conversion at 593 K (see Figs. 1 and 3), this means that factors other than the molybdenum surface exposure and molybdenum sulphidation degree might influence the catalyst activity in HDS of DBT. One of these factors could be sulphidation degree of promoter since it follows the same trend as activity of binary samples after HDS of DBT (Ni–Mo > Ru–Mo > Pd–Mo). The absence of a similar correlation after HDS of gas-oil points to a lower catalyst sulphidation with CS_2/gas-oil mixture, as discussed above.

It is commonly accepted that HDS reactions are catalysed by metal sulphides. In an attempt to rank the performance and to see if there is some kind of periodic trend in the silica–alumina-supported monometallic catalysts, the HDS activity of DBT, normalised to the amounts of metal sulphide, is plotted in Fig. 8 as a function of the position of the metal in periodic table (activity is expressed as millimole of DBT converted per millimole of transition metal sulphide per hour). In the particular case of Ir sample, activity was normalised to Ir^0 because no sulphide phase was observed (cf. Table 2). The intrinsic activity increased with increasing metal position in the periodic table (Mo < Ru < Ir < Pd). This trend is different from the volcano-shaped curves reported by Pecoraro and Chianelli [11] for bulk TMS with Ru being the most active. A common feature between the performance of ASA-supported catalysts and the bulk TMS is that the silica–alumina-supported Mo and Ni monometallics were found to be relatively inactive. In the Ni sample, nickel reacts during the preparation steps through

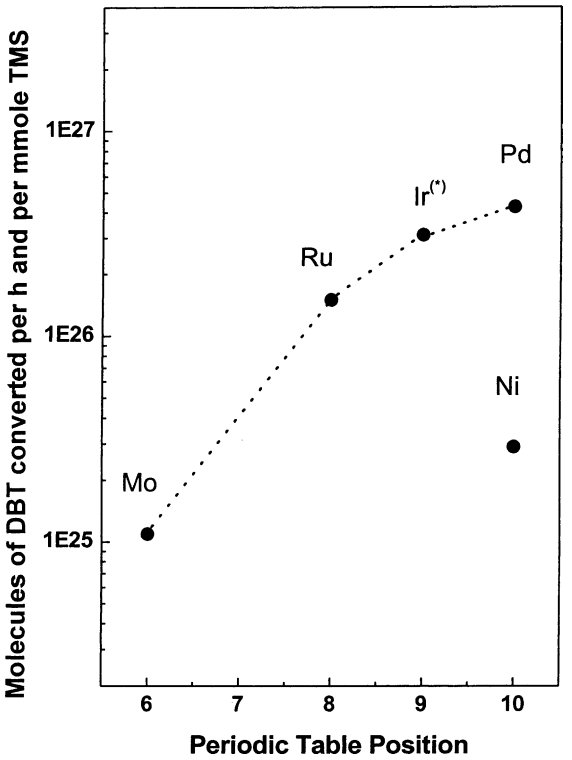

Fig. 8. Activity of monometallic M/ASA (M = Mo, Ru, Ir, Pd and Ni) catalysts after HDS of DBT at 593 K normalised per millimole TMS vs. periodic table position of catalytic promoters: (*) as calculated for Ir^0 phase.

solid-state reaction with support components forming a nickel hydrosilicate phase, more than one atomic layer thick. In the case of Mo catalyst, the experimental Mo/Si surface ratio (Table 3) is much higher than the theoretical Mo/Si ratio calculated according to the Kerkhoff–Moulijn model [47], in which monolayer coverage of the carrier surface is assumed. This finding, which is consistent with the strong decrease of BET specific area of the carrier upon Mo incorporation to the support, indicates Mo-enrichment on the external surface. The formation of the MoO_3 phase of crystal size 8.7 nm and $Mo_{17}O_{47}$ phase of crystal size 9.3 nm was confirmed by XRD measurements.

The comparison of HYD selectivity as a function of the reaction temperature in Fig. 4 reveals that silica–alumina-supported Mo species, and its binary Pd–Mo and Ru–Mo counterparts, follow a different behaviour than the other monometallic or bimetallic catalysts. The Mo sample shows a low S/Mo ratio after HDS of DBT (S/Mo = 0.88), indicating a partial sulphidation of molybdenum species. In the rim model–edge model proposed by Chianelli and Daage [48], the rim layers at the top and bottom of MoS_2 layers are active sites for HYD pathway whereas the HDS pathway occurs on both rim and edge sites. Assuming this model, the temperature dependence of HYD selectivity observed for Mo sample (Fig. 4) suggests that the number of rim sites increase with increasing reaction temperature. In other words, the structure of the anchored molybdenum species undergoes some changes upon increasing reaction temperature. On the contrary, its bimetallic Ni–Mo counterpart exhibits good HDS activity (Figs. 1 and 2) but a low HYD selectivity, which did not change with reaction temperature pointing to a good stability of this catalyst. This important difference comes from the great tendency of Ni^{2+} ions to diffuse toward the interface (nickel hydrosilicate is formed), whereas Mo remains on its top thus minimising the interaction of molybdenum species with the support surface. Additionally, the location of molybdenum species may also change as a consequence of the two-step impregnation method employed in the preparation of the bimetallic systems. As a general rule, some redissolution of Mo may occur during Ni incorporation in a consecutive impregnation step, and the solubilised molybdenum fraction being forced to precipitate on the top catalyst surface at the end of the drying process. Accordingly, the proportion of exposed Ni atoms is expected to be lower in the bimetallic Ni–Mo catalyst than in the monometallic Ni sample.

The influence of the promoter on the behaviour of molybdenum in a reducing environment is revealed by TPR profiles. The enhancement in the reducibility of the supported MoO_3 layer by adding small amounts of Ni, Ru and Pd is illustrated by the shift of ca. 50 K in the reduction temperature of MoO_3 phase (Table 1), and agrees with previous observations for alumina- and silica-supported Mo catalysts [30,31]. However, only for the bimetallic Ru–Mo and Ni–Mo samples is there an expected correlation between the reducibility of the oxidic precursor and the HDS activity of the sulphided samples [29]. This is not true for the Pd–Mo which displays lower HDS activity, comparable to that of Mo monometallic catalyst. Although there is no definite explanation, it may be speculated that Pd mainly contributes to hydrogenation but only a

little, if any, to HDS reaction. If a comparison is made in the HYD selectivity in the HDS reaction of DBT over the monometallic catalysts (see Fig. 4), Pd shows a higher HYD ability than the other monometallic catalysts along the temperature range explored. It was also reported in a previous work by using dynamic low temperature oxygen chemisorption measurements that both monometallic Mo and bimetallic Pd–Mo display a similar dispersion degree [14]. This may suggest that Pd in Pd–Mo catalyst is not effective as a promoter due its poorer dispersion and low surface exposure.

4.3. Catalyst acidity

Fig. 9 displays data of total DBT conversion at 593 K on monometallic and bimetallic catalysts as a function of Brønsted-to-Lewis acidity ratio. For the bimetallic catalysts, the conversion of DBT increased progressively with Brønsted-to-Lewis acidity ratio. For the monometallic catalysts, the absence of such a correlation might be masked by the effect of support since the blank silica–alumina substrate displayed substantial activity in HDS reactions of DBT and gas-oil. The similar activity of the silica–alumina support and the Mo sample should be understood assuming that some –SH groups could be developed on the silica–alumina surface, as it was observed for γ-alumina and NaY zeolite [49]. Their formation results from heterolytic dissociation of H_2S that is present in the feed during a catalytic run after HDS [50]. Thus, as pointed out by Topsøe et al. [1], the presence of Brønsted acidity and its role in HDS reaction over sulphided molybdenum-containing catalysts is still not clear. Other important question is if acidity of catalysts might influence HYD selectivity of catalysts during HDS reaction. Literature data indicate that hydrogenation selectivity is in general enhanced over more acidic carriers [51]. However, in this study there is no correlation between the HYD selectivity during HDS of DBT (Fig. 4) and the Lewis-to-Brønsted ratios of the catalysts (Table 3). In particular, the hydrogenation selectivity of Ni–Mo catalyst is lower than that of Pd–Mo, whereas the Lewis-to-Brønsted ratio follows the opposite trend. To reconcile this, a tentative explanation is that the number of coordinated unsaturation rim sites of MoS_2 might be different for the two catalysts [48].

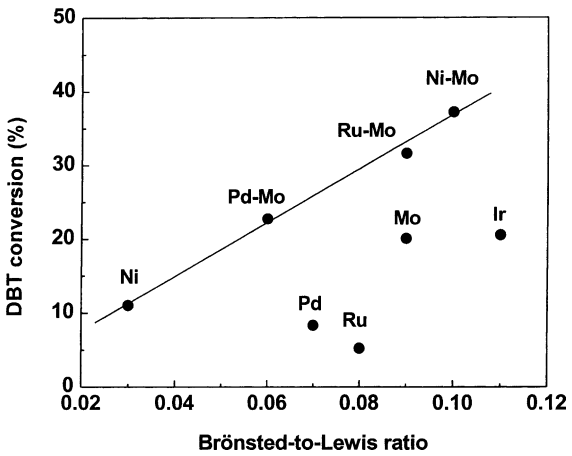

Fig. 9. Influence of Brønsted-to-Lewis acidity ratio on DBT conversion at 593 K.

5. Conclusions

A variety of noble and seminoble metals (Ru, Pd, Ir, Ni) supported on ASA and Mo/ASA catalysts have been used in the hydrodesulphurization of DBT and gas-oil under experimental conditions which approach industrial practice. On the basis of the data presented above, the following conclusions can be drawn: (i) the catalysts prepared showed similar response in the hydrodesulphurization reactions of DBT and gas-oil, and appeared more active with DBT than with gas-oil feed; (ii) irrespective of the feed used, the bimetallic M–Mo catalysts were more active than the monometallic catalysts, and Ni–Mo was the best catalyst although somewhat less active than the commercial $CoMo/Al_2O_3$ sample; and (iii) the consecutive impregnation of calcined Mo/ASA catalyst with precursor solution followed by calcination enhances molybdenum surface exposure in binary samples. As a consequence, the temperature of reduction of MoO_3 to molybdenum suboxides is decreased.

Acknowledgements

BP and RMN acknowledge financial support from the Spanish Ministry of Science and Technology (Ramon and Cajal Program) and the European Social

Fund (ESF) (I3P-PC2001-2 Program), respectively. We thank Mr. M. Toural Quiroga in the assistance in gas-oil HDS tests.

References

[1] H. Topsøe, B.S. Clausen, F.E. Massoth, in: J.R. Anderson, M. Boudart (Eds.), Hydrotreating Catalysis, Science and Technology, vol. 11, Springer, Berlin, 1996.
[2] P.T. Vasudevan, J.L.G. Fierro, Catal. Rev.-Sci. Eng. 38 (2) (1996) 161.
[3] A. Ishihara, K. Shirouchi, T. Kabe, Chem. Lett. 589 (1993).
[4] M. Breysse, J.L. Portefaix, M. Vrinat, Catal. Today 10 (1991) 489.
[5] C.V. Cáceres, J.L.G. Fierro, J. Lázaro, A. López Agudo, J. Soria, J. Catal. 122 (1990) 113.
[6] J. Ramirez, S. Fuentes, G. Diaz, M. Vrinat, M. Breysse, M. Lacroix, Appl. Catal. 52 (1989) 211.
[7] G. Muralidhar, F.E. Massoth, J. Shabtai, J. Catal. 85 (1984) 44.
[8] F. Luck, Bull. Soc. Chem. Belg. 100 (11–12) (1991) 781.
[9] R. Frety, P.N. da Silva, M. Guenin, Appl. Catal. 57 (1990) 99.
[10] F.E. Massoth, G. Muralidhar, J. Shabtai, J. Catal. 85 (1984) 53.
[11] T.A. Pecoraro, R.R. Chianelli, J. Catal. 67 (1981) 430.
[12] R. Navarro, B. Pawelec, J.L.G. Fierro, P.T. Vasudevan, Recent Research Developments in Catalysis, Research Signpost, 1996, p. 1.
[13] R. Navarro, B. Pawelec, J.L.G. Fierro, P.T. Vasudevan, J.F. Cambra, P.L. Arias, Appl. Catal. A 137 (1996) 269.
[14] R. Navarro, B. Pawelec, J.L.G. Fierro, P.T. Vasudevan, Appl. Catal. A 148 (1996) 23.
[15] P.T. Vasudevan, J.L.G. Fierro, B. Pawelec, in: T. White, D. Sun (Eds.), Advances in Environmental Materials, Materials Research Society, Singapore, June 2001.
[16] H. Makishima, Y. Tanaka, Y. Kato, S. Kure, H. Shimada, N. Matsubayashi, A. Nishijima, M. Nomura, Catal. Today 29 (1–4) (1996) 267.
[17] H.R. Reinhoudt, R. Troost, S. van Schalkwijk, A.D. van Langeveld, S.T. Sie, H. Schulz, D. Chadwick, J. Cambra, V.H.J. de Beer, J.A.R. van Veen, J.L.G. Fierro, J.A. Moulijn, Stud. Surf. Sci. Catal. 106 (1997) 237.
[18] H.R. Reinhoudt, R. Troost, A.D. van Langeveld, S.T. Sie, J.A.R. van Veen, J.A. Moulijn, Fuel Process. Technol. 61 (1–2) (1999) 133.
[19] H.R. Reinhoudt, R. Troost, S. van Schalkwijk, A.D. van Langeveld, S.T. Sie, J.A.R. van Veen, J.A. Moulijn, Fuel Process. Technol. 61 (1–2) (1999) 117.
[20] W.R.A.M. Robinson, J.A.R. van Veen, V.H.J. de Beer, R.A. van Santen, Fuel Process. Technol. 61 (1–2) (1999) 103.
[21] W.R.A.M. Robinson, J.A.R. van Veen, V.H.J. de Beer, R.A. van Santen, Fuel Process. Technol. 61 (1–2) (1999) 89.
[22] E.J.M. Hensen, P.J. Kooyman, Y. van deer Meer, A.M. van der Kraan, V.H.J. de Beer, J.A.R. van Veen, R.A. van Santen, J. Catal. 199 (2001) 224.
[23] T.I. Koranyi, M. Dobrovolszky, T. Koltai, K. Matusek, Z. Paál, P. Tetenyi, Fuel Process. Technol. 61 (1–2) (1999) 55.
[24] R. Barth, A. Ramachandran, J. Catal. 125 (1990) 467.
[25] M.L. Vrinat, Appl. Catal. 6 (1983) 137.
[26] M.J. Girgis, B.C. Gates, Ind. Eng. Chem. Res. 30 (1991) 2021.
[27] C.G. Frye, A.W. Weitkamp, J. Chem. Eng. Data 14 (1969) 372.
[28] S.J. Gregg, K.S.W. Sing (Eds.), Adsorption, Surface Area and Porosity, 2nd ed., Academic Press, London, 1982.
[29] Y.-W. Chen, W.-C. Hsu, C.-S. Lin, B.-C. Kang, S.-T. Wu, L.-J. Leu, J.-C. Wu, Ind. Eng. Chem. Res. 29 (1990) 1830.
[30] F.E. Massoth, J. Catal. 36 (1975) 164.
[31] V.H.J. de Beer, C. Bevelander, T.H.M. van Sint Fiet, P.G.A. Werter, C.H. Amberg, J. Catal. 43 (1976) 68.
[32] T.-C. Chang, J.-J. Chen, C.-T. Yeh, J. Catal. 96 (1985) 51.
[33] X.L. Seoane, N.S. Fígoli, P.C. L'Argentiere, J.A. González, A. Arcoya, Catal. Lett. 47 (1997) 213.
[34] B. Scheffer, P. Molhoek, J.A. Moulijn, Appl. Catal. A 46 (1989) 11.
[35] B. Mile, D. Stirling, M.A. Zammitt, A. Lovell, M. Webb, J. Catal. 114 (1988) 217.
[36] J. Zielinski, J. Catal. 76 (1982) 157.
[37] V.L. Barrio, P.L. Arias, J.F. Cambra, M.B. Güemez, B. Pawelec, J.L.G. Fierro, Appl. Catal. A 248 (2003) 211.
[38] A.J. Hegedüs, K. Sasvári, J. Neugebauer, Z. Anorg. Allg. Chem. 293 (1957) 56.
[39] D.K. Lambiev, T.T. Tomova, G.V. Samsonov, Powder Metall. Int. 4 (1972) 17.
[40] F. Pinna, M. Signoretto, G. Strukul, A. Benedetti, M. Malentacchi, N. Pernicone, J. Catal. 155 (1995) 166.
[41] D. Briggs, M.P. Seah, Practical Surface Analysis by Auger and X-ray Photoelectron Spectroscopy, Wiley, Chichester, UK, 1983.
[42] P.C.H. Mitchell, C.E. Scott, J.P. Bonnelle, J.G. Grimblot, J. Catal. 107 (1987) 482.
[43] J.A. De los Reyes, S. Göbölös, M.L. Vrinat, M. Breysse, Catal. Lett. 5 (1990) 17.
[44] P. Dufresne, J. Grimblot, J.P. Bonelle, J. Phys. Chem. 85 (1981) 2344.
[45] E.P. Parry, J. Catal. 2 (1963) 371.
[46] M. Nagai, T. Kabe, J. Catal. 81 (1983) 440.
[47] F.P.J.M. Kerkhoff, J.A. Moulijn, J. Phys. Chem. 83 (1979) 1612.
[48] R.R. Chianelli, M. Daage, Proceedings of the 202nd National ACS Meeting, Abstract CATL 38, August 25–30, 1991.
[49] A.V. Deo, I.G. Dalla Lana, H.W. Habgood, J. Catal. 21 (1971) 270.
[50] G. Berhault, M. Lacroix, M. Breysse, F. Maugé, J.-C. Lavalley, H. Nie, L. Qu, J. Catal. 178 (1998) 555.
[51] E. Dhainaut, H. Charcosset, C. Gachet, L. de Mourgues, Appl. Catal. 2 (1982) 75.